Requirement of translocated lysosomal V1 H^+-ATPase for activation of membrane acid sphingomyelinase and raft clustering in coronary endothelial cells

Ming Xu, Min Xia, Xiao-Xue Li, Wei-Qing Han, Krishna M. Boini, Fan Zhang, Yang Zhang, Joseph K Ritter, and Pin-Lan Li

Address: Department of Pharmacology and Toxicology, Medical College of Virginia, Virginia Commonwealth University. 1220 East Broad Street, P.O. Box 980613, Richmond, VA 23298, Tel. 804 828-4793; Fax: 804 828-2117

Correspondence to: Pin-Lan Li, MD, PhD; E-Mail: pli@vcu.edu

Running title: Lysosomal V1 H^+-ATPase and raft clustering

Abstract

Acid sphingomyelinase (ASM) mediates the formation of membrane rafts (MRs) redox signalosomes in a process that depends on a local acid microenvironment in coronary arterial endothelial cells (CAECs). However, it remains unknown how this local acid microenvironment is formed and maintained. The present study hypothesized that lysosomal V1 H^+-ATPase provides a hospitable acid microenvironment for activation of ASM when lysosomes traffic and fuse into cell membrane. By confocal microscopy, local pH change significantly affected MRs with more fluorescent patches under low pH. Correspondingly, the ASM product, ceramide, increased locally in the cell membrane. ESR assay showed that local pH increase significantly inhibited NADPH oxidase-mediated production of $O_2^{\cdot-}$ in CAECs. Direct confocal microscopy demonstrated that Fas ligand resulted in localized areas of decreased pH around CAEC membranes. The inhibitors of both lysosomal fusion and H^+-ATPase apparently attenuated FasL-caused pH decrease. V1 H^+-ATPase accumulation and activity on cell membranes were substantially suppressed by the inhibitors of lysosomal fusion or H^+-ATPase. These results for the first time provide direct evidence that translocated lysosomal V1 H^+-ATPase critically contributes to the formation of local acid microenvironment to facilitate activation of ASM and consequent MR aggregation, forming MR redox signalosomes and mediating redox signaling in CAECs.

Introduction

Lipid rafts (LRs), which consist of dynamic assemblies of cholesterol and lipids with saturated acyl chains in the membrane of cells (Bollinger et al., 2005), play an essential role in signal transduction (Cherukuri *et al.*, 2001; Brown, 2006; Allen *et al.*, 2007; Yamazaki *et al.*, 2007). Since many studies indicated that raft formation is not driven solely by lipids, but also by protein interactions (Pike, 2006), it is more appropriate that these rafts are referred to as membrane rafts (MRs)(Zhang and Li, 2010). The clustered MRs can recruit or aggregate various signaling molecules to form platforms that initiate receptor-mediated trans-membrane signal transduction in a variety of mammalian cells (Gupta and DeFranco, 2003; Li *et al.*, 2007; Yamazaki *et al.*, 2007; Kuebler *et al.*, 2010; Li *et al.*, 2010). For example, we demonstrated that MR clustering on the arterial endothelium could recruit some redox signaling molecules, including NADPH oxidase subunits and Rac GTPase, to impair endothelial function by enhanced production of reactive oxygen species (ROS) (Zhang et al., 2006).

Our recent studies have indicated that MR-redox signaling in coronary arterial endothelial cells (CAECs) was related to the increased activity of lysosomal acid sphingomyelinase (ASM), which hydrolyzes membrane-bound sphingomyelin into the bioactive lipid, ceramide (Zhang et al., 2007). Lysosome-associated vesicle transportation or trafficking of ASM from the abluminal compartment to the cell membrane is a prerequisite for ASM activation (Jin et al., 2008a). In addition, ASM is characterized by working optimally at acidic pH (Schuchman, 2010). Thus, it is expected that an acid microenvironment around the cell membrane is critical to the formation of MR redox signaling by ASM activation. However, the mechanism by which the acid environment is formed remains obscure.

It is generally accepted that some factors, including proton leak, ClC chloride channels or Na^+/K^+-ATPase participate in the regulation of extracellular or intracellular pH. Among these factors, the activity of the vacuolar H^+-ATPase is regarded as a primary factor of pH regulation (Zou et al., 2010). H^+-ATPase is a multi-subunit trans-membrane complex responsible for pumping protons from the cytoplasm to the lumen of organelles or outside the cell (Forgac, 2007). As a consequence, H^+-ATPase plays a role in acidifying the extracellular medium or

controlling the cytoplasmic pH (Li et al., 1999). On the lysosomal membrane, H^+-ATPase functions to acidify the vesicle compartmental environment, thereby facilitating the activities of various acid hydrolases. When endothelial cells (ECs) are stimulated by death-receptor agonists such as Fas ligand (FasL) or TNF-α, lysosomal vesicles traffic or migrate to the cell membrane (Bao et al., 2010b). It has been reported that phagosome acidification occurs by direct recruitment of H^+-ATPase derived from lysosomes (Sun-Wada et al., 2009), which provides us an idea that H^+-ATPase may function to provide a local acid environment around the cell membrane after lysosomes fuse to the plasma membrane. Therefore, a quite reasonable hypothesis is that lysosomal trafficking upon FasL stimulation results in H^+-ATPase accumulation in the cell membrane, which pumps protons outside the cells and provides a hospitable environment for the ASM, thereby promoting the clustering of MRs.

The present study was designed to test this hypothesis. First, we analyzed the effects of local pH change on MR raft clustering and NADPH oxidase activity in CAECs. Second, we tested whether local endogenous pH around ECs was changed by FasL stimulation, using the pH indicator dye, OG488, added to the tissue chamber with cells immobilized in matrigel. Then, in addition to the use of the inhibitors of lysosome fusion, some inhibitors targeting H^+-ATPase were applied to examine their effects on FasL-induced change in local pH. Furthermore, we investigated if H^+-ATPase protein can be translocated into cell membrane accompanying with lysosomal fusion into cell membrane. All these experiments attempted to demonstrate that the translocated lysosomal H^+-ATPase exerts a critical local influence on the extracellular pH, which facilitates the formation and activation of MR redox-signaling signalosomes that are associated with ASM in coronary endothelial cells.

Results

Effects of pH changes on local ceramide production and MRs clusters

Fluorescence microscopy is prevalently used to study cell MRs. For example, fluorophores conjugated to cholera-toxin B-subunit can bind to the raft constituent ganglioside GM1. In present study, Al488-CtxB was used to label MRs. Under resting condition, there was only some diffuse fluorescent staining on the cell membrane stained by Al488-CtxB (Figure 1A, Ctrl.), indicating an even distribution of single MRs without clusters. When the cells were incubated with FasL for 15 min, large fluorescent dots or patches were detected on the cell

membrane. These fluorescent patches indicate the possible formation of MRs clusters or macrodomains. In addition, MR clustering and colocalization with ceramide was significantly blocked by the MR disruptor, methyl-β-cyclodextrin (MCD) (Supplemental Figure 1), which made sure that MR clustering is involved in the stimulation of FasL. To test the role of pH changes, the medium pH of the culture medium was adjusted to 5.5, 6.0, 6.5, 7.0, and 7.5, respectively, before addition of FasL. It was found that MRs clusters increased when the pH of the bath solution was lowered. Figure 1B shows that the percentage of cluster positive cells stained by Al488-CtxB after FasL treatment significantly increased compared with control at all pH levels. The magnitude of the increases in MRs clusters was much higher when the pH of the bath solution was lower than 6.0. In addition, our previous studies showed that the frequency histogram of CtxB staining was not right shifted to higher fluorescence intensity, when CAECs were treated with FasL (*Antioxid Redox Signal. 2010;12(6):703-712*). Thus, FasL mainly produced MRs clustering under different pH value without the alteration of the amount of MRs on the cell membrane. In the colocalization study using Al488-CtxB and a Texas red–conjugated anti-ceramide antibody, ceramide production was found locally in MRs in response to FasL when the pH of the bath solution was in the range of 5.5-6.5 (Figure 1C). But when the pH increased to 7.0 or 7.5, the colocalization was not detected. Figure 1D summarizes the results of the co-staining of CAECs by Al488-CtxB and Texas red–conjugated anti-ceramide antibody. After the cells were treated with FasL, the percentage of cell with the colocalization of MRs and ceramide staining dramatically increased when pH in the bath solution was lower than 6.5, but not increased significantly at pH equal to or higher than 7.0.

Using flow cytometry with anti-ceramide antibody, we found that the frequency histogram of membrane surface ceramide was shifted to higher fluorescence intensity in a pH-dependent manner with a maximum production of ceramide at pH of 6.0 (Figure 2A). These results were summarized in Figure 2B. In addition, through observation with forward and side scatter, and viability analysis *with* ViaCount reagent, pH change was found to not affect cell size, granularity or cell viability (Figure2C). LC/MS analysis of ceramide confirmed this pH-dependent difference in ceramide production on the cell surface in response to FasL stimulation (Figure 3A). Moreover, FasL-induced ceramide production was dependent on

ASM, because inhibition of ASM blocked the FasL-induced increase in ceramide production (Figure 3B).

Extracellular pH changes affected FasL-induced $O_2^{-\cdot}$ production of the CAECs

In previous studies, we demonstrated that FasL-induced MRs clustering resulted in the formation of redox signaling platforms associated with increased NADPH oxidase activity, and production of $O_2^{-\cdot}$ (Bao et al., 2010a). Therefore, we measured $O_2^{-\cdot}$ as a functional parameter in response to FasL stimulation at different pHs. In these experiments, NADPH-dependent $O_2^{-\cdot}$ production was measured by CMH trapping after incubation of the cells with NADPH as substrate. The SOD-inhibitable fraction of the signal specifically reflected NADPH-dependent $O_2^{-\cdot}$ production. Figure 4A depicts representative changes in ESR spectrometric curve recorded under control and FasL-treated conditions. It was clear that the spectra of CMH-trapped $O_2^{-\cdot}$ markedly increased in response to FasL with a higher production rate at lower pH of the bath solution. As summarized in Figure 4B, a rapid increase in $O_2^{-\cdot}$ production stimulated by FasL was observed in a pH-dependent manner compared to control. At extracellular pH of 6.0, FasL-induced $O_2^{-\cdot}$ production reached maximum. When pH increased to 7.5, FasL-induced $O_2^{-\cdot}$ production was significantly reduced compared to that at pH 6.0. In addition, compared with control, FasL markedly increased the $O_2^{-\cdot}$ production, which was inhibited after the pretreatment with membrane raft inhibitor MCD (Supplemental Figure 2). It made sure that MR clustering is involved in the effect of FasL.

Role of lysosomal enzymes in MRs

To demonstrate the contribution of lysosome-derived enzymes to pH-dependent MRs, we first tested the involvement of lysosomes in the fluorescent patches. FasL stimulated MRs and ceramide aggregation. When the lysosome fusion inhibitor, vacuolin-1, was used to pretreat the cells, FasL-induced MRs and ceramide aggregation were completely blocked. Similarly, when the lysosomal enzyme, ASM, was inhibited by its siRNA or inhibitor, Ami, both MRs and aggregated ceramide induced by FasL were no longer observed even though the pH of the bath solution was maintained at 6.0. Lysosomal H^+-ATPase subunit of V1 sector (V1 H^+-ATPase) siRNA or its inhibitor also substantially inhibited FasL-induced MRs and ceramide

aggregation. These results are summarized in Figure 5A, showing that the colocalization coefficient of MRs and ceramide was significantly increased after stimulation of the cells with FasL. Vacuolin-1 is a non-specific inhibitor of lysosomal fusion, and bafilomycin A1 (Baf) is a macrolide antibiotic that specifically inhibits the V0 subunit of H^+-ATPase. When the cells were pretreated with vacuolin-1, the ASM siRNA or ASM inhibitor-Ami, or the lysosomal V1 H^+-ATPase siRNA or Baf, FasL failed to induce any MRs and ceramide aggregation in the membrane of CAECs.

In addition, membrane fraction flotation analysis detected positive expression of flotillin-1, a component and marker of MRs, in fractions 3 to 5, which were referred to as MRs fractions previously (Shao et al., 2003). Figure 5B shows that V1 H^+-ATPase could be detected in membrane raft fractions in CAECs. A marked increase in V1 H^+-ATPase protein in MR microdomains was observed when CAECs were stimulated by FasL. This increase was significantly attenuated by pretreatment with V1 H^+-ATPase siRNA.

H^+-ATPase in FasL-induced changes in extracellular pH and intracellular $O_2^{-\cdot}$

In these experiments, DHE was loaded into the cells to detect the level of intracellular $O_2^{-\cdot}$ level and OG488 was added into matrigel solution to monitor extracellular pH changes around the cells. Measurement of $O_2^{-\cdot}$ reflects FasL-induced raft-redox signaling as we demonstrated in previous studies (Bao et al., 2010a). Figure 6A presents typical fluorescent images showing changes in extracellular pH (from blue to yellow) and intracellular $O_2^{-\cdot}$ (from light red to dark red within the cell). A rapid change in pH outside the cells in response to FasL was observed, as shown in acquired images at time points of 0, 3, 6 and 12 min following addition of FasL. In the presence of V1 H^+-ATPase siRNA or its inhibitor Baf, FasL no longer increased intracellular or extracellular fluorescence. Figure 6B presents the summarized data illustrating pH changes and $O_2^{-\cdot}$ production in response to FasL under control condition and with H^+-ATPase inhibitor or its siRNA. Under the control condition or when CAECs were treated with scrambled sRNA, FasL time-dependently increased OG488 fluorescence, meaning reduction in pH outside these cells, while intracellular $O_2^{-\cdot}$ levels increased in parallel. However, these changes in extracellular pH and intracellular $O_2^{-\cdot}$ levels induced by FasL were substantially attenuated by pretreatment of the cells with either H^+-ATPase inhibitor, Baf, or its siRNA. In addition, MCD

significantly inhibited FasL-induced changes in extracellular pH and intracellular $O_2^{-\cdot}$ production in CAECs, which suggested that MR clustering induced by FasL is involved in these changes in extracellular pH and intracellular $O_2^{-\cdot}$ levels (Supplemental Figure 3).

Lysosome fusion required for FasL-induced changes in extracellular pH and intracellular $O_2^{-\cdot}$

To demonstrate whether the FasL-induced extracellular pH decrease or intracellular $O_2^{-\cdot}$ increase are associated with lysosome fusion, we tested the effects of siRNA or chemical lysosome fusion inhibitors on the changes in extracellular pH and intracellular $O_2^{-\cdot}$. Tetanus toxin is a special inhibitor of SNARE (Soluble N-ethylmaleimide-sensitive factor attachment protein receptor) inhibitor. As shown by the typical fluorescence images presented in Figure 7A, lysosome fusion inhibition by tetanus toxin, vacuolin-1 or tSNARE siRNA (Vamp siRNA) almost completely blocked FasL-induced reduction of extracellular pH and increase in intracellular $O_2^{-\cdot}$ production compared to that observed under control condition or after treatment with scrambled sRNA. Figure 7B summarizes these results. Under the control condition or when CAECs were treated with scrambled sRNA, FasL time-dependently increased OG488 fluorescence, meaning the pH outside the cells decreased, while the intracellular $O_2^{-\cdot}$ level increased. This parallel decrease in extracellular pH and increase in intracellular $O_2^{-\cdot}$ level induced by FasL was significantly attenuated by inhibition of lysosome fusion using either tetanus toxin, vacuolin-1 or Vamp siRNA.

Lysosome fusion-dependent translocation of H^+-ATPase

As shown in Figure 8A, after stimulation with FasL the frequency histogram of H^+-ATPase as measured by cytometry was right shifted to higher fluorescence intensity, suggesting recruitment of the protein into the cell membrane. In the presence of lysosome fusion inhibitor, vacuolin-1 or tetanus toxin, the aggregation of V1 H^+-ATPase protein was effectively suppressed. These results are summarized in Figure 8B. The percentage of positive-staining cells with anti-V1 H^+-ATPase was significantly increased by FasL, an effect that was substantially attenuated by vacuolin-1 or tetanus toxin. It appears that V1 H^+-ATPase proteins are translocated to the cell membrane after the activation by FasL and that lysosomal fusion

mediates this translocation. In FRET experiments, V1 H^+-ATPase was found translocated into the cell membrane from lysosomes because the FRET (blue images) between V1 H^+-ATPase and ganglioside GM1 (CtxB labeling) or ASM increased upon FasL stimulation (Figure 9A). These results are summarized in Figure 9B, showing that the FRET efficiency between V1 H^+-ATPase and ASM or GM1 significantly increased in response to FasL stimulation. Pretreatment of these CAECs with lysosome fusion inhibitor, vacuolin-1 and V1 H^+-ATPase siRNA remarkably decreased the FRET efficiency.

Lysosome fusion-dependent H^+-ATPase activity on the membrane of CAECs

Bafilomycin sensitive H^+-ATPase activity on the CAEC membrane is shown in Figure 10A. H^+-ATPase activity was significantly enhanced upon FasL stimulation for 15 minutes. In the presence of vacuolin-1, the FasL-induced enhancement of H^+-ATPase activity was significantly blocked. Similar results were obtained by another lysosome fusion inhibitor, tetanus toxin or V1 H^+-ATPase siRNA. Interestingly, V1 H^+-ATPase siRNA had no effects on H^+-ATPase activity in the absence of FasL stimulation. It is likely that the surface activity as measured in their assay reflects an activity other than that of the H^+-ATPase to which the siRNA is directed. Further, cell surface biotinylation assay showed that V1 H^+-ATPase protein was increased by 59.5% on the cell membrane when BCAECs were treated with FasL, which suggested that about 59.5% of the total V1 H^+-ATPase may be externalized to cell membrane due to FasL treatment. In addition, ASM or lysosomal-associated membrane protein 1(Lamp-1) are regarded as control of the re-localization of lysosomal protein to the cell surface, and it was found that the intensity ratio of ASM or Lamp-1 to transferrin receptor increased by 67.1 % or 47.7%, respectively, on the cell member. (Figure 10B, C).

Discussion

In the present study, it was firstly found that MR clustering was decreased when pH was turned to neutral or slightly alkaline condition. Consistent with such changes in MR clustering, the colocalization of MR and ASM product, ceramide, was reduced when extracellular pH increased. In addition, the results from flow cytometry and ceramide quantification further demonstrated that FasL-induced MR clustering contributed to the production of ceramide in

the cell membrane at low extracellular pH level. Moreover, both confocal and flow cytometric analyses showed that pH 6.0 was an optimum condition for the intensive MR cluster formation. These results suggest that ASM-associated MR clustering is dependent upon a low pH microenvironment around the ECs.

Our previous studies showed that MR clustering is an important mechanism determining the trafficking and aggregation of NADPH oxidase subunits in the cell membrane of endothelial cells (Jin et al., 2008b). In addition, lysosome-targeted ASM is able to traffic to and become exposed on the cell-membrane surface, which may lead to MRs clustering and NADPH oxidase activation in CAECs (Bao et al., 2010a). In this process, it remained unclear as to the role of local extracellular pH change on the activity of NADPH oxidase. The present study showed that that an acidic pH was important for the activation of lysosomal enzymes and MR cluster formation. This action of pH on MR cluster formation had a profound effect on NADPH oxidase activity (Mantegazza et al., 2008). As measured by ESR, NADPH oxidase activity stimulated by FasL in CAECs was highly sensitive to extracellular pH, which is consistent with MR clustering that varied with different pH. Although there are a number of reports indicating that NADPH oxidase may be working in a pH-dependent manner with an optimum near pH 6.0 (Henderson, 1998; DeCoursey *et al.*, 2001; Schwarzer *et al.*, 2004), these studies did not associate such pH dependence with MR clustering.

One of the important findings from the present study is that local pH changes around the cell membrane of CAECs upon stimulation by FasL are the determinant for MR clustering and formation of MR redox signalosomes. The synchronous change between local extracellular pH change and intracellular $O_2^{\cdot -}$ production further demonstrated that MR clustering due to pH changes is associated with NADPH oxidase activity. This local acidic microenvironment is important for the activation of the MR-redox signaling in these cells, as shown by intracellular $O_2^{\cdot -}$ production.

The next question we tried to answer was what mechanism mediates the FasL-induced pH decrease outside these CAECs. In previous studies, we identified that lysosomes were fused with the cell membrane upon FasL stimulation, leading to the translocation of ASM (Jin et al., 2008a), (Bao et al., 2010b). Moreover, lysosomal trafficking was importantly involved in MR clustering in EC membrane, leading to the formation of signaling platforms (Jin et al., 2008a).

The present study further demonstrated that the fusion and function of lysosomes was involved in the FasL-induced pH decrease and MR-redox activation in response to FasL, as shown by the blocking effect of the lysosomal fusion inhibitors on the FasL-induced pH decrease. In addition, we found that MT-depolymerising reagents nocodazole can inhibit the fluorescent destaining of lysosomal dye FM2-10, which suggested that microtubule plays a role in lysosomal relocation to cell membrane in response to FasL (Supplemental Figure 4). To our knowledge, these results for the first time provide evidence that lysosomal fusion leads to a local pH reduction and thereby determines MR clustering and redox signaling activation.

To further explore the mechanisms mediating the formation of local acidic environment for ASM around cell membrane during FasL stimulations, we addressed the role of H^+-ATPase. Given the fact that H^+-ATPase pumps protons from the cytoplasma into lysosomes (Jefferies et al., 2008; Tabata et al., 2008), outward proton flux may occur because the inner member of lysosomes often faces outside the cells. Additionally, some factors are reported to that participate in the regulation of pH. For example, it has been reported that the generation of $O_2^{\cdot -}$ by the NADPH oxidase is accompanied by the efflux of H^+ ions through H^+ channel, which acts as the charge compensation pathway for the electrogenic generation of $O_2^{\cdot -}$ (Henderson, 1998). Also, interference of α4 isoform of Na^+/K^+-ATPase with ouabain causes a pH decline of the sperm cytoplasm through functionally coupling to the Na^+/H^+ exchanger (Jimenez *et al.*, 2010) and PKC-mediated phosphorylation of rat α1 Na^+/K^+-ATPase alters pH in COS cells (Belusa *et al.*, 1997). However, the present study demonstrated that bafilomycin A1 resulted in a failure of FasL to reduce the extracellular local pH. V1 H^+-ATPase siRNA was also found to eliminate the FasL-induced pH decrease outside CAECs. Thus, our data suggest that V1 H^+-ATPase rather than NADPH oxidase-associated H^+ channel or Na^+/K^+-ATPase coupling with Na^+/H^+ exchanger plays a major role in H^+ transportation in EC membrane.

Recent studies have indicated that ASM can be acidified in lysosomes depending on luminal pH prior to fusion of the vesicles. It was reported that in hepatocytes, hyperosmotic exposure induces an almost instantaneous acidification of ASM containing endosomal compartment, which is followed by an increase in the intracellular ceramide concentration (Reinehr and Haussinger, 2007; Lang *et al.*, 2011). Moreover, inhibition of the vacuolar-type H^+-ATPase abolishes not only endosomal acidification and subsequent ceramide generation,

but also hyperosmotically induced generation of ROS by NADPH oxidase. The present study suggested that when lysosome fuses with cell membrane, translocated lysosomal V1 H^+-ATPase provides an acid environment, which maintains the activation of membrane acid sphingomyelinase to magnify the production of ceramide. Taken together, these data suggest a model that ASM is activated in the lysosome to initialize the ceramide production in the lysosome; once ASM is translocated in the plasma membrane, translocated lysosomal V1 H^+-ATPase provides a micro-environment with acidic pH which is critical to sustain the ASM activity for production of large amount ceramide and consequent formation of ceramide-enriched membrane platforms.

Additional experiments were performed to determine whether H^+-ATPase stems from translocated lysosomes induced by FasL. Using flow cytometry, it was confirmed that this FasL-induced translocation of V1 H^+-ATPase was mainly stemmed from lysosomes because V1 H^+-ATPase positive stained cells was substantially blocked by vacuolin-1 and tetanus toxin. By confocal microscopy, V1 H^+-ATPase was also found to be translocated into the MR clusters when CAECs were stimulated by FasL, which was significantly inhibited by treatment with either vacuolin-1 or V1 H^+-ATPase siRNA. FRET analysis demonstrated that V1 H^+-ATPase and ASM are very closely localized after they are translocated to the cell MR areas. This suggests that lysosomal V1 H^+-ATPase is not only aggregated in the cell membrane upon FasL stimulations, but also is assembled into an MR signalosome complex to function as a signaling platform. It was reported that MR like domains also plays a role in regulating the activity of the H^+-ATPase pump (Lafourcade *et al.*, 2008). It is plausible that there is feed-forward loop for H^+-ATPase aggregation in membrane raft and membrane raft clustering. In this model, upon stimulation, lysosomal fusion with plasma membrane results in exposure of H^+-ATPase in plasma membrane, which is crucial for ASM activation, ceramide production and consequent formation of ceramide-enriched membrane platforms. H^+-ATPase aggregation in MR platform may enhance acidic micro-environment around this platform and thus enhances ASM activity, which promotes the formation of larger ceramide-enriched signaling platforms and amplifies raft-associated signals. The activity of H^+-ATPase activity is critical for the activity of ASM to produce ceramide-enriched MR clusters and consequent redox signaling platforms. This enhanced H^+-ATPase activity by FasL treatment was indeed

demonstrated by biochemical analysis. Further, it was suggested that the membrane H^+-ATPase activity in these cells is due to the its translocation via lysosome fusion.

In conclusion, FasL stimulation leads to a local acid microenvironment around CAEC membrane, which facilitates the activity of ASM and enables consequent formation of MR-redox signal platforms. The activation of translocated V1 H^+-ATPase via lysosome fusion serves as a proton pump and functions to keep such local acid region for the activity of ASM leading to ceramide production and MR clustering, which promotes the formation of membrane redox signalosomes and thereby importantly participates in the regulation of endothelial function in the coronary circulation.

Materials and Methods

Cell culture

Primary cultures of bovine CAECs were obtained as we described previously (Zhang et al., 2006) (Jin et al., 2008b). All studies were performed with CAECs of 2–4 passages.

RNA interference of ASM, Vamp-2 and H^+-ATPase

siRNAs were designed with *BLOCK-iT™ RNAi Designer* (Invitrogen Life Science). The DNA target sequence for H^+-ATPase siRNA is: 5'-CACAGCGAGUUGGUUGGAGAGAUUA-3', ASM-siRNA is: 5'-AAGGCCGTGAGTTTCTACCT-3', Vamp-2 siRNA: 5'-CAUCAUCGUUUACUUCAGCUCUUAA-3' and the scrambled small RNA (AATTCTCCGAACGTGTCACGT) has been confirmed as nonsilencing double-stranded RNA and was used as control in the present study. Transfection of siRNA was performed using the QIAGEN TransMessengerTM transfection kit according to the manufacturer's instructions. In view of the role of the H^+-ATPase V1 subunit on traffic (Oehlke *et al.*, 2011), V1 subunit E1 mRNA (LOCUS: NM_001079613) and its cDNA was chosen to design H^+-ATPase siRNA. V1 H^+-ATPase siRNA was confirmed to be effective in silencing H^+-ATPase gene and protein expression through Western bolt, PCR and immunocytochemistry (Supplemental Figure5). The siRNAs of ASM and Vamp-2 have been confirmed to be effective in silencing ASM and Vamp-2 gene expression in our lab (Zhang *et al.*, 2007; Han *et al.*, 2011).

Confocal microscopy of the colocalization of MR clusters and ceramide

For dual-staining detection of the colocalization of MR marker with ceramide or V1 H^+-ATPase, the CAECs were first incubated with Alexa488-Cholera-toxin B (Al488-CtxB), as described previously (Zhang et al., 2006), and then as needed, with mouse anti-ceramide IgM antibody (1:200; Alexis Biochemicals, San Diego, CA), which was followed by Texas red-conjugated anti-mouse secondary antibody (Molecular Probes, Eugene, OR). Then, the colocalizations were visualized by confocal microscopic analysis. In addition, CtxB clusters positive cells were counted from total 50 cells under fluorescent microscope. Then, the percent changes of CtxB clusters positive cells were calculated.

Flow-cytometric analysis of ceramide generation and H^+-ATPase translocation on cell membrane

The expression of ceramide and V1 H^+-ATPase on the cell membrane was also assessed by flow cytometry. As described previously (Varsano et al., 1998), CAECs were harvested and washed with PBS, and then blocked with 1% BSA for 10 min at 4°C. Cell viability assessed by trypan blue staining was always greater than 96%. After two washes, the pellet was added to 100 ml PBS and incubated with goat anti-V1 H^+-ATPase IgG (1:200) or mouse anti-ceramide IgM antibody (1:200), followed by incubation with FITC-labeled rabbit anti-goat secondary antibody (BD Biosciences; 1:500) or Texas red-conjugated anti-mouse secondary antibody (Molecular Probes, Eugene, OR). Stained cells were run on a Guava Easycyte Mini Flow Cytometry System (Guava Technologies, Hayward, CA) and analyzed with Guava acquisition and analysis software (Guava Technologies).

Liquid chromatography electrospray ionization tandem mass spectrometry (LC–ESI– MS) for quantitation of ceramide

The separation, identification, and quantitation of ceramide in CAECs was performed by LC-ESI-MS. The HPLC was equipped with a binary pump, a vacuum degasser, a column heater, and an autosampler (Waters, Milford, MA, USA). The HPLC separation was performed at 70°C on a reverse phase C18 Nucleosil AB column (5 μm, 70 mm×2 mm i.d.) from Macherey Nagel (Düren, Germany). The mobile phase was a gradient mixture formed as

described (Fillet et al., 2002). The cell lipids were extracted according to previous studies (Yi et al., 2004). To avoid any loss of lipids, the extraction procedure was performed using siliconized glassware. MS detection was carried out using a Quattro II quadrupole mass spectrometer (Micromass, Altrincham, England) operating under MassLynx 3.5 and configured with a Z-spray electrospray ionization source. Source conditions were described as previously (Fillet et al., 2002).

ESR detection of $O_2^{\cdot-}$

For detection of the $O_2^{\cdot-}$ production dependent on NADPH oxidase, cells were gently collected and resuspended with modified Krebs–Hepes buffer containing deferoximine (100 μmol/L; Sigma, St. Louis, MO, USA) and diethyldithiocarbamate (5 μmol/L; Sigma). These mixtures containing 1×10^6 cells were subsequently mixed with 1 mM of the $O_2^{\cdot-}$-specific spin trap 1-hydroxy-3- methoxycarbonyl-2,2,5,5-tetramethylpyrrolidine (CMH) in the presence or absence of manganese- dependent SOD (200 U/ml; Sigma). The mixtures were then loaded into glass capillaries and immediately analyzed for $O_2^{\cdot-}$ formation kinetics for 10 min in a Miniscope MS200 ESR spectrometer (Magnettech Ltd., Berlin, Germany) as described (Jin et al., 2008b). The ESR settings were as follows: biofield, 3350; field sweep, 60 G; microwave frequency, 9.78 GHz; microwave power, 20 mW; modulation amplitude, 3 G; 4096 points of resolution; receiver gain, 50 for cells. The results were expressed as the fold changes of the treatment group versus the control.

Flotation of membrane MR fractions

CAECs pretreated with vehicle or V1 H^+-ATPase siRNA were stimulated by FasL (10 ng/ml) for 15 min. To isolate LR fractions from the cell membrane, these cells were lysed in 1.5 ml MBS buffer containing (in micromoles per liter) morpholinoethane sulfonic acid, 25; NaCl, 150; EDTA, 1; PMSF, 1; Na_3VO_4, 1; and a mixture of protease inhibitors and 1% Triton X-100 (pH 6.5). Cell extracts were homogenized by 5 passages through a 25-gauge needle. Then, homogenates were adjusted with 60% OptiPrep Density Gradient medium (Sigma, St. Louis, MO, USA) to 40% and overlaid with an equal volume (4.5mL) of discontinuous 30%–5% OptiPrep Density Gradient medium. Samples were centrifuged at 32,000 rpm for 24 h at 4°C

using a SW32.1 rotor. Fractions were collected from the top to bottom. Then, proteins in each fraction were precipitated by adding an equal volume of 30% trichloroacetic acid and incubating for 30 min on ice. Precipitated proteins were spun down by centrifugation at 13,000 rpm at 4°C for 15min. The protein pellet was carefully washed twice with cold acetone, air dried, and resuspended in 1 mol/L Tris–HCl (pH 8.0) for Western. In addition, Na^+/K^+-ATPase, a cell membrane protein not considered to cluster with MRs, was used as a negative control in this experiment (Figure5B).

Simultaneous confocal microscopic analysis of intracellular $O_2^{-\cdot}$ and extracellular pH in CAECs

To measure intracellular $O_2^{-\cdot}$ production in isolated vascular endothelial cells, we used a DNA-binding assay for $O_2^{-\cdot}$, which oxidizes exogenously added DHE to produce a strong red fluorescence. In these experiments, isolated CAECs (1×10^6 cells/well) were seeded into a 35-mm dish and incubated overnight to attach to the bottom of the wells. The cells were then pretreated with bafilomycin A1 (Baf, 100 nM, Sigma), tetanus toxin (TT, 10nM, Sigma), vacuolin-1(10μM, Sigma), amitriptyline (Ami, 20μM, Sigma) or siRNA of ASM, Vamp-2 or V1 H^+-ATPase before treating with FasL. On the day of experiments, the culture medium was first discarded, and CAECs were washed twice with PBS buffer followed by addition of 1 mL PBS containing DHE (10 μM; Invitrogen). After 30 min at room temperature, the DHE solution was discarded, and the cells were washed twice with fresh PBS and then overlaid with Matrigel containing OG488 (1mM). The change of OG488 fluorescent intensity was recorded in Pseudo color, which shows blue to green, then to yellow with increasing fluorescent intensity (Baader *et al.*, 2002). The staining of DHE for intracellular $O_2^{-\cdot}$ and OG488 for extracellular pH was visualized after treatment with FasL, respectively, using an Olympus scanning confocal microscope (Olympus, Tokyo, Japan) at excitation/emission of 480/610 nm and 495/524 nm. The merged image was shown as the final result. DHE and OG488 fluorescent intensity was analyzed with Fluoview version 5.0 software. The ratio of fluorescent intensity to that at basal level was quantified to show $O_2^{-\cdot}$ level and pH change.

Fluorescence resonance energy transfer measurement

To determine the molecular complex in MR clusters, CAECs were stained with FITC-labeled anti-V1 H^+-ATPase antibody and then with tetramethylrhodamine isothiocyanate (TRITC)- labeled CtxB, Alexa488-labeled anti-V1 H^+-ATPase antibody or Alexa555-labeled anti-ASM antibody. These cells were then visualized using confocal microscopy. An acceptor bleaching protocol was employed to measure the fluorescence resonance energy transfer (FRET) efficiency (Van Munster *et al.*, 2005; Nieminen *et al.*, 2007; Jin *et al.*, 2008a; Bao *et al.*, 2010b). After pre-bleaching images were taken, the laser intensity at an excitation wavelength of the acceptor (TRITC or Alex555) was increased from 50 to 98 W/cm^2 and continued to excite the sample cells for 2 min to bleach the acceptor fluorescence. After the excitation intensity was adjusted back to 50 W/cm^2, the post-bleaching image was then taken. The FRET images were obtained by subtraction of the pre-bleaching image from the post-bleaching image and are shown in blue color. The FRET efficiency was calculated as described previously (Van Munster *et al.*, 2005; Nieminen *et al.*, 2007; Jin *et al.*, 2008a; Bao *et al.*, 2010b).

Assay for H^+-ATPase activity

The method for determination of H^+-ATPase activity is a modification of the assay for H^+-ATPase activity in microdissected tubule segments (Tojo et al., 1994). ATPase activity was measured by a fluorometric method in which ATP hydrolysis was coupled to oxidation of NADH. Baf was used as a specific inhibitor of vacuolar H^+-ATPase. CAECs (1×10^6 cells/well) were seeded into a 35-mm dish and pretreated with vacuolin-1 prior to FasL stimulation for 15 min. Then, the CAECs were harvested and resuspended in assay buffer containing (in mM) 100 NaCl, 66.7 NH_4Cl, 3.7 $MgC1_2$, 2 $CaC1_2$, 50 imidazole, 5 glucose, and 0.05% BSA. To each sample was added 20 μl of reaction solution 1 with or without bafilomycin. Reaction solution 1 contained (in mM): 100 NaCl, 66.7 NH_4Cl, 3.7 $MgCl_2$, 50 imidazole, 3.3 disodium ATP, 0.6 phosphoenopyruvate, 7.5 sodium azide, 12 ouabain, 1 EDTA, and 9.6 U/ml pyruvate kinase. All samples were divided into two groups, one without and the other with 30 nM bafilomycin. In the second group, reaction solution 1 containing either 30 nM bafilomycin was added. After addition of reaction solution 1, the samples were incubated in a shaking water bath at 37°C for

40 min. The reactions were stopped by boiling the samples for 3 min. The amount of pyruvate generated during the first stage of the assay was determined by reacting the samples with 2.5 μM NADH and 6 U/ml lactate dehydrogenase in 1,100 μl of 0.1 N potassium phosphate buffer (reaction solution 2), and the amount of NADH oxidized by pyruvate was measured by fluorometry. The excitation and emission wavelengths for NADH were 340 and 460 nm, respectively.

The bafilomycin-sensitive ATPase activity was defined as the difference in activity determined in the absence and presence of bafilomycin. The H^+-ATPase activity was expressed as pmol of ADP generated per minute per 10^6 cells. The H^+-ATPase assay was performed under maximum reaction rate (Vmax) conditions, as all reactants in the assay were added in considerable excess and ATP was being continuously regenerated during the assay. The only limiting factor was the generation of ADP from ATP by ATPases during the first stage of the assay. There was a 1:1 stoichiometric relationship between ADP formation during the first stage of the assay and NADH oxidation during the second stage of the assay. Therefore, a change in enzyme activity reflects a change in Vmax, and changes in the kinetic properties of the enzyme because of putative changes in Michaelis constant for the substrate (ATP) or cofactors (Mg^{2+}) would not be detected under these conditions.

Cell surface biotinylation assay for expression for H^+-ATPase protein

As described previously (Perrotta et al., 2010), Cells (1×10^6 cells/well) were stimulated with 10ng/ml FasL at the indicated times in culture medium at 37 °C. Stimulation was stopped with ice-cold PBS. Cells were washed twice with PBS and then incubated twice with 0.5 mg/ml Sulfo-NHS-LC-Biotin in DMEM without serum for 10 min at 4 °C. After washing with serum-free DMEM for 10 min and three times with PBS for 5 min at 4 °C, cells were solubilized in lysis buffer (10 mM Tris, 150 mM NaCl, 1 mM EDTA, 0.1% SDS, 1% Triton X-100 with protease inhibitor mixture, pH 7.4) for 30 min at 4 °C. Lysates were then centrifuged for 5 min at 1,500×*g*, and streptavidin beads were added to the supernatant to isolate cell membrane proteins. After incubation of the mixture for 16 h at 4 °C, biotin-streptavidin beads complexes were sedimented at 13,000 rpm for 3 min. The supernatant was used as control, and, after two washes with PBS, bead-bound proteins were

denatured in Laemmli buffer and analyzed by SDS-PAGE followed by Western blotting with the anti-V1 H^+-ATPase, anti-lamp-1, or anti-ASM Ab. Lamp-1 and ASM is regarded as positive control. Transferrin receptor was a conserved membrane protein as a loading control in this study. Cell surface exposure of protein was normalized to 25 μg of total lysate for each sample.

Statistics

Data are presented as the mean ± SE. Significant differences between and within multiple groups were examined using ANOVA for repeated measures, followed by Duncan's multiple-range test. A Students' t-test was used to detect significant differences between two groups. $P<0.05$ was considered statistically significant.

Acknowledgements

This work was supported by National Heart, Lung, and Blood Institute Grants HL057244, HL0765316 and HL091464.

References

Allen, J.A., Halverson-Tamboli, R.A., and Rasenick, M.M. (2007). Lipid raft microdomains and neurotransmitter signalling. Nat Rev Neurosci *8*, 128-140.

Baader, A.P., Buchler, L., Bircher-Lehmann, L., and Kleber, A.G. (2002). Real time, confocal imaging of Ca(2+) waves in arterially perfused rat hearts. Cardiovasc Res *53*, 105-115.

Bao, J.X., Jin, S., Zhang, F., Wang, Z.C., Li, N., and Li, P.L. (2010a). Activation of membrane NADPH oxidase associated with lysosome-targeted acid sphingomyelinase in coronary endothelial cells. Antioxid Redox Signal *12*, 703-712.

Bao, J.X., Xia, M., Poklis, J.L., Han, W.Q., Brimson, C., and Li, P.L. (2010b). Triggering role of acid sphingomyelinase in endothelial lysosome-membrane fusion and dysfunction in coronary arteries. Am J Physiol Heart Circ Physiol *298*, H992-H1002.

Belusa, R., Wang, Z.M., Matsubara, T., Sahlgren, B., Dulubova, I., Nairn, A.C., Ruoslahti, E., Greengard, P., and Aperia, A. (1997). Mutation of the protein kinase C phosphorylation site on rat alpha1 Na+,K+-ATPase alters regulation of intracellular Na+ and pH and influences cell shape and adhesiveness. J Biol Chem *272*, 20179-20184.

Bollinger, C.R., Teichgraber, V., and Gulbins, E. (2005). Ceramide-enriched membrane domains. Biochim Biophys Acta *1746*, 284-294.

Brown, D.A. (2006). Lipid rafts, detergent-resistant membranes, and raft targeting signals. Physiology (Bethesda) *21*, 430-439.

Cherukuri, A., Dykstra, M., and Pierce, S.K. (2001). Floating the raft hypothesis: lipid rafts play a role in immune cell activation. Immunity *14*, 657-660.

DeCoursey, T.E., Cherny, V.V., DeCoursey, A.G., Xu, W., and Thomas, L.L. (2001). Interactions between NADPH oxidase-related proton and electron currents in human eosinophils. J Physiol *535*, 767-781.

Fillet, M., Van Heugen, J.C., Servais, A.C., De Graeve, J., and Crommen, J. (2002). Separation, identification and quantitation of ceramides in human cancer cells by liquid chromatography-electrospray ionization tandem mass spectrometry. J Chromatogr A *949*, 225-233.

Forgac, M. (2007). Vacuolar ATPases: rotary proton pumps in physiology and pathophysiology. Nat Rev Mol Cell Biol *8*, 917-929.

Gupta, N., and DeFranco, A.L. (2003). Visualizing lipid raft dynamics and early signaling events during antigen receptor-mediated B-lymphocyte activation. Mol Biol Cell *14*, 432-444.

Han, W.Q., Xia, M., Zhang, C., Zhang, F., Xu, M., Li, N.J., and Li, P.L. (2011). SNARE-mediated rapid lysosome fusion in membrane raft clustering and dysfunction of bovine coronary arterial endothelium. Am J Physiol Heart Circ Physiol *301*, H2028-2037.

Henderson, L.M. (1998). Role of histidines identified by mutagenesis in the NADPH oxidase-associated H+ channel. J Biol Chem *273*, 33216-33223.

Jefferies, K.C., Cipriano, D.J., and Forgac, M. (2008). Function, structure and regulation of the vacuolar (H+)-ATPases. Arch Biochem Biophys *476*, 33-42.

Jimenez, T., Sanchez, G., Wertheimer, E., and Blanco, G. (2010). Activity of the Na,K-ATPase alpha4 isoform is important for membrane potential, intracellular Ca2+, and pH to maintain motility in rat spermatozoa. Reproduction *139*, 835-845.

Jin, S., Yi, F., Zhang, F., Poklis, J.L., and Li, P.L. (2008a). Lysosomal targeting and trafficking of acid sphingomyelinase to lipid raft platforms in coronary endothelial cells. Arterioscler Thromb Vasc Biol *28*, 2056-2062.

Jin, S., Zhang, Y., Yi, F., and Li, P.L. (2008b). Critical role of lipid raft redox signaling platforms in endostatin-induced coronary endothelial dysfunction. Arterioscler Thromb Vasc Biol *28*, 485-490.

Kuebler, W.M., Yang, Y., Samapati, R., and Uhlig, S. (2010). Vascular barrier regulation by PAF, ceramide, caveolae, and NO - an intricate signaling network with discrepant effects in the pulmonary and systemic vasculature. Cell Physiol Biochem *26*, 29-40.

Lafourcade, C., Sobo, K., Kieffer-Jaquinod, S., Garin, J., and van der Goot, F.G. (2008). Regulation of the V-ATPase along the endocytic pathway occurs through reversible subunit association and membrane localization. PLoS One *3*, e2758.

Lang, P.A., Graf, D., Boini, K.M., Lang, K.S., Klingel, K., Kandolf, R., and Lang, F. (2011). Cell volume, the serum and glucocorticoid inducible kinase 1 and the liver. Z Gastroenterol *49*, 713-719.

Li, P.L., Zhang, Y., and Yi, F. (2007). Lipid raft redox signaling platforms in endothelial dysfunction. Antioxid Redox Signal *9*, 1457-1470.

Li, X., Becker, K.A., and Zhang, Y. (2010). Ceramide in redox signaling and cardiovascular diseases. Cell Physiol Biochem *26*, 41-48.

Li, Y.P., Chen, W., Liang, Y., Li, E., and Stashenko, P. (1999). Atp6i-deficient mice exhibit severe osteopetrosis due to loss of osteoclast-mediated extracellular acidification. Nat Genet *23*, 447-451.

Mantegazza, A.R., Savina, A., Vermeulen, M., Perez, L., Geffner, J., Hermine, O., Rosenzweig, S.D., Faure, F., and Amigorena, S. (2008). NADPH oxidase controls phagosomal pH and antigen cross-presentation in human dendritic cells. Blood *112*, 4712-4722.

Nieminen, J., Kuno, A., Hirabayashi, J., and Sato, S. (2007). Visualization of galectin-3 oligomerization on the surface of neutrophils and endothelial cells using fluorescence resonance energy transfer. J Biol Chem *282*, 1374-1383.

Oehlke, O., Martin, H.W., Osterberg, N., and Roussa, E. (2011). Rab11b and its effector Rip11 regulate the acidosis-induced traffic of V-ATPase in salivary ducts. J Cell Physiol *226*, 638-651.

Perrotta, C., Bizzozero, L., Cazzato, D., Morlacchi, S., Assi, E., Simbari, F., Zhang, Y., Gulbins, E., Bassi, M.T., Rosa, P., and Clementi, E. (2010). Syntaxin 4 is required for acid sphingomyelinase activity and apoptotic function. J Biol Chem *285*, 40240-40251.

Pike, L.J. (2006). Rafts defined: a report on the Keystone Symposium on Lipid Rafts and Cell Function. J Lipid Res *47*, 1597-1598.

Reinehr, R., and Haussinger, D. (2007). Hyperosmotic activation of the CD95 system. Methods Enzymol *428*, 145-160.

Schuchman, E.H. (2010). Acid sphingomyelinase, cell membranes and human disease: lessons from Niemann-Pick disease. FEBS Lett *584*, 1895-1900.

Schwarzer, C., Machen, T.E., Illek, B., and Fischer, H. (2004). NADPH oxidase-dependent acid production in airway epithelial cells. J Biol Chem *279*, 36454-36461.

Shao, D., Segal, A.W., and Dekker, L.V. (2003). Lipid rafts determine efficiency of NADPH oxidase activation in neutrophils. FEBS Lett *550*, 101-106.

Sun-Wada, G.H., Tabata, H., Kawamura, N., Aoyama, M., and Wada, Y. (2009). Direct recruitment of H+-ATPase from lysosomes for phagosomal acidification. J Cell Sci *122*, 2504-2513.

Tabata, H., Kawamura, N., Sun-Wada, G.H., and Wada, Y. (2008). Vacuolar-type H(+)-ATPase with the a3 isoform is the proton pump on premature melanosomes. Cell Tissue Res *332*, 447-460.

Tojo, A., Guzman, N.J., Garg, L.C., Tisher, C.C., and Madsen, K.M. (1994). Nitric oxide inhibits bafilomycin-sensitive H(+)-ATPase activity in rat cortical collecting duct. Am J Physiol *267*, F509-515.

Van Munster, E.B., Kremers, G.J., Adjobo-Hermans, M.J., and Gadella, T.W., Jr. (2005). Fluorescence resonance energy transfer (FRET) measurement by gradual acceptor photobleaching. J Microsc *218*, 253-262.

Varsano, S., Rashkovsky, L., Shapiro, H., and Radnay, J. (1998). Cytokines modulate expression of cell-membrane complement inhibitory proteins in human lung cancer cell lines. Am J Respir Cell Mol Biol *19*, 522-529.

Yamazaki, S., Iwama, A., Morita, Y., Eto, K., Ema, H., and Nakauchi, H. (2007). Cytokine signaling, lipid raft clustering, and HSC hibernation. Ann N Y Acad Sci *1106*, 54-63.

Yi, F., Zhang, A.Y., Janscha, J.L., Li, P.L., and Zou, A.P. (2004). Homocysteine activates NADH/NADPH oxidase through ceramide-stimulated Rac GTPase activity in rat mesangial cells. Kidney Int *66*, 1977-1987.

Zhang, A.Y., Yi, F., Jin, S., Xia, M., Chen, Q.Z., Gulbins, E., and Li, P.L. (2007). Acid sphingomyelinase and its redox amplification in formation of lipid raft redox signaling platforms in endothelial cells. Antioxid Redox Signal *9*, 817-828.

Zhang, A.Y., Yi, F., Zhang, G., Gulbins, E., and Li, P.L. (2006). Lipid raft clustering and redox signaling platform formation in coronary arterial endothelial cells. Hypertension *47*, 74-80.

Zhang, C., and Li, P.L. (2010). Membrane raft redox signalosomes in endothelial cells. Free Radic Res *44*, 831-842.

Zou, X.P., Chen, M., Zhang, X.Q., Zhang, B., Cao, J., and Luo, H.S. (2010). Expression of Vacuolar H+-ATPases and the intracellular pH values in three adenocarcinoma cell lines of digestive system. Cell Mol Biol (Noisy-le-grand) *56 Suppl*, OL1268-1275.

Figure Legends

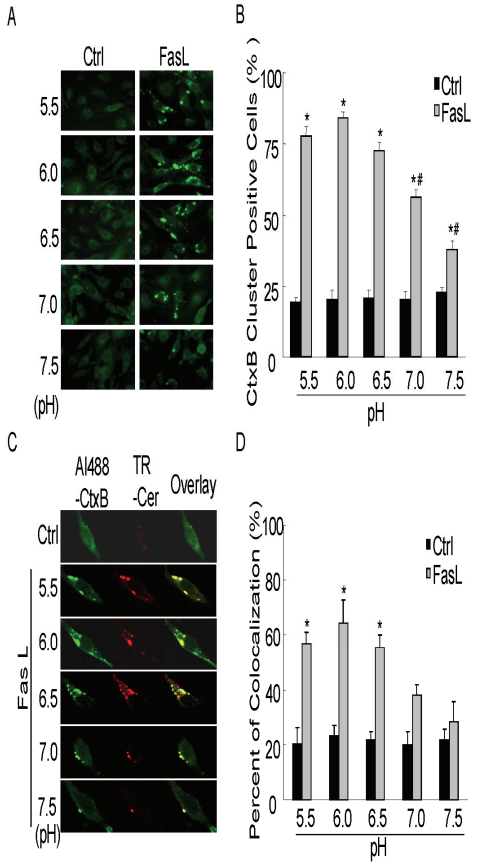

Figure 1. Effects of pH change on the colocalization of CtxB staining fluorescent patches and ceramide. (A) Representative confocal microscopic images of CAECs stained by Al488-CtxB. (B) Summarized effects showing that FasL significantly increased the percentage of CtxB cluster positive cells stained by Al488-CtxB at pH 5.5, 6.0, 6.5, 7.0, and 7.5. (C) Representative confocal microscopic images of the colocalization of CtxB staining patches and ceramide in FasL-treated CAECs at different pH. Al488-CtxB is shown as a pseudo green color on the left; Texas red-conjugated anti-ceramide shown as red color in the middle; and overlaid images shown on the right. Yellow spots in the overlaid images were defined as patches of the colocalization in CtxB staining patches and ceramide. The images are representatives from six separated batches of CAECs. (D) Percentage changes in positive cells co-stained by Al488-CtxB and anti-ceramide antibody during FasL stimulation (n=6, $^{*}P<0.05$ *vs.* control; $^{\#}P<0.05$ *vs.* pH=6.0 group).

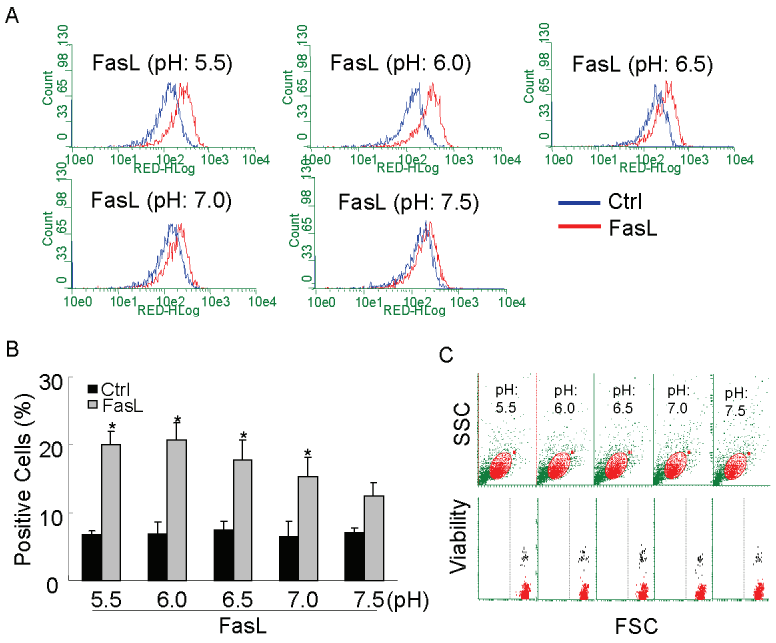

Figure 2. Measurements of ceramide in bovine CAECs by flow cytometry. (A) Frequency histogram of ceramide in control and FasL-treated cells exposed to pH 5.5, 6.0, 6.5, 7.0, and 7.5. (B) The percentage of ceramide positive-staining cells increased due to FasL treatment under different pH condition. At pH 6.0, the percentage reached the maximum (n=6, $^{*}P<0.05$ *vs.* control). (C) The top flow cytometric plot shows that there was no significant change of forward and side scatter under different pH conditions, which suggested that the treatment had no effects on cell size or granularity. The lower plot shows cell viability measured by flow cytometry. Cells were stained by ViaCount reagent. Viable cells appear at the bottom of plot, and dead cells were at the top. The results show that the viability was no less than 95% under different pH conditions.

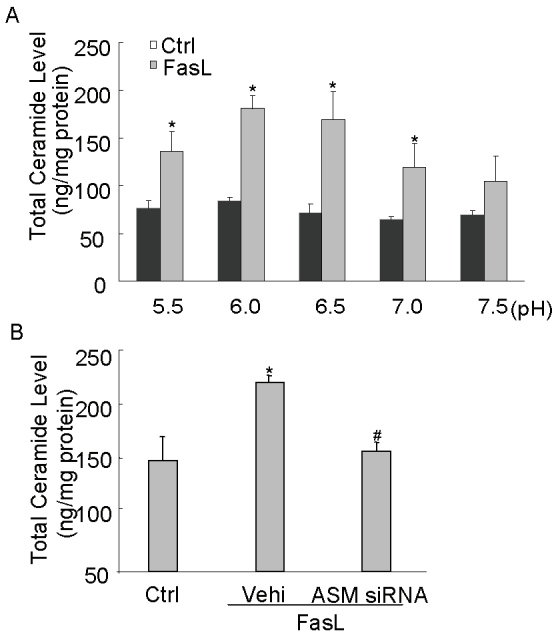

Figure 3. Measurement of ceramide concentration by LC-ESI-MS. (A) Ceramide concentration in CAECs was increased due to FasL treatment under different pH conditions. Moreover, ceramide reached the maximum at pH 6.0. (B) ASM siRNA transfection significantly blocked the FasL-induced increase in ceramide production. (n=4, $^{*}P<0.05$ *vs.* control; $^{\#}P<0.05$ *vs.* only FasL-treated group).

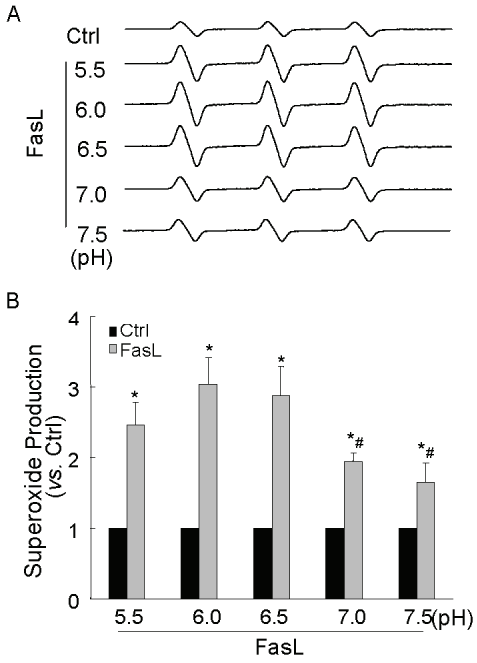

Figure 4. ESR spectrometric analysis of O_2.- production in bovine CAECs stimulated by FasL. (A) Representative ESR spectrographs of O_2.- trapped by CMH using NADPH as substrate. (B) Summarized data showing that O_2.- production following FasL treatment (10 ng/ml) markedly increased, and gradually decreased as the extracellular pH increased from 6.0 to 7.5 (n=6, $^{*}P<0.05$ *vs.* control; $^{\#}P<0.05$ *vs.* pH=6.0 group).

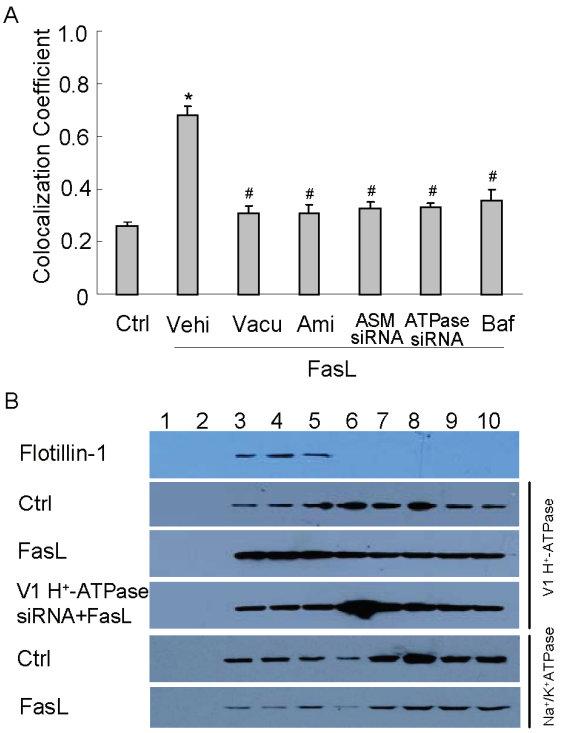

Figure 5. Effects of lysosome fusion inhibition on the CtxB staining fluorescent patches and ceramide. (A) Percentage changes in positive cells co-stained by Al488-CtxB and anti-ceramide antibody in FasL-stimulated CAECs pretreated with lysosome fusion inhibitor, vacuolin-1 (10 μM), ASM inhibitor, Ami (20 μM), ASM siRNA, V1 H^+-ATPase siRNA and its inhibitor, Baf (100 nM). (n = 6, $^*P<0.05$ *vs.* control; $^\#P<0.05$ *vs.* only FasL-treated group). (B) Distribution and localization of H^+-ATPase as a MR redox platform on the membrane in CAECs treated with FasL alone or with FasL after pretreatment of V1 H^+-ATPase siRNA. Fractions 3 to 5 were designated as MRs as indicated by the marker protein, flotillin-1. The blot pattern for H^+-ATPase represents 4 individual experiments. Na^+/K^+-ATPase could also be detected in membrane raft fractions. However, no marked increase in the Na^+/K^+-ATPase protein in MR microdomains was observed in FasL treated CAECs.

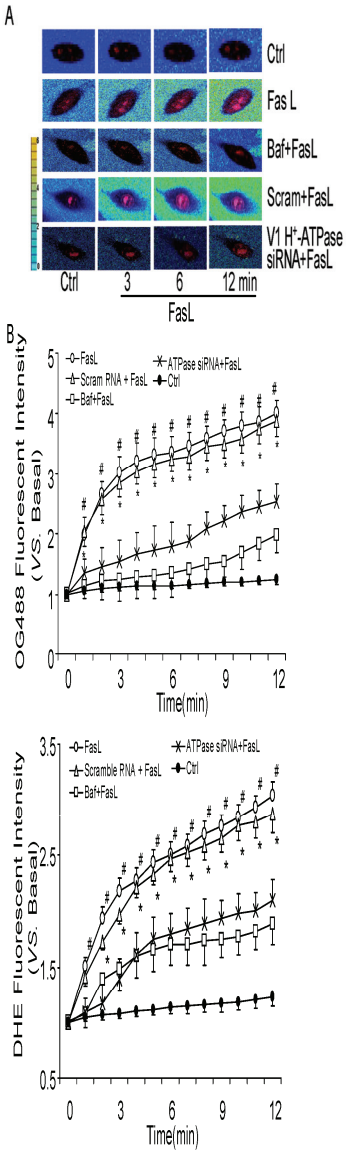

Figure 6. Role of lysosomal H^+-ATPase in extracellular pH and O_2.- production in bovine CAECs. (A) Typical merged images of OG488 and DHE fluorescence using an Olympus scanning confocal microscope at excitation/emission of 480/610 nm and 495/524 nm. The change of OG488 fluorescent intensity was recorded with pseudo color, which shows blue to green, then to yellow with increasing fluorescent intensity. (B) Summarized data showing that treatments with Baf (100nM) or V1 H^+-ATPase siRNA significantly inhibited FasL-induced changes in extracellular pH and intracellular O_2.- production in CAECs (n=6, $^*P<0.05$ *vs.* V1 H^+-ATPase siRNA-treated group; $^\#P<0.05$ *vs.* Baf-treated group).

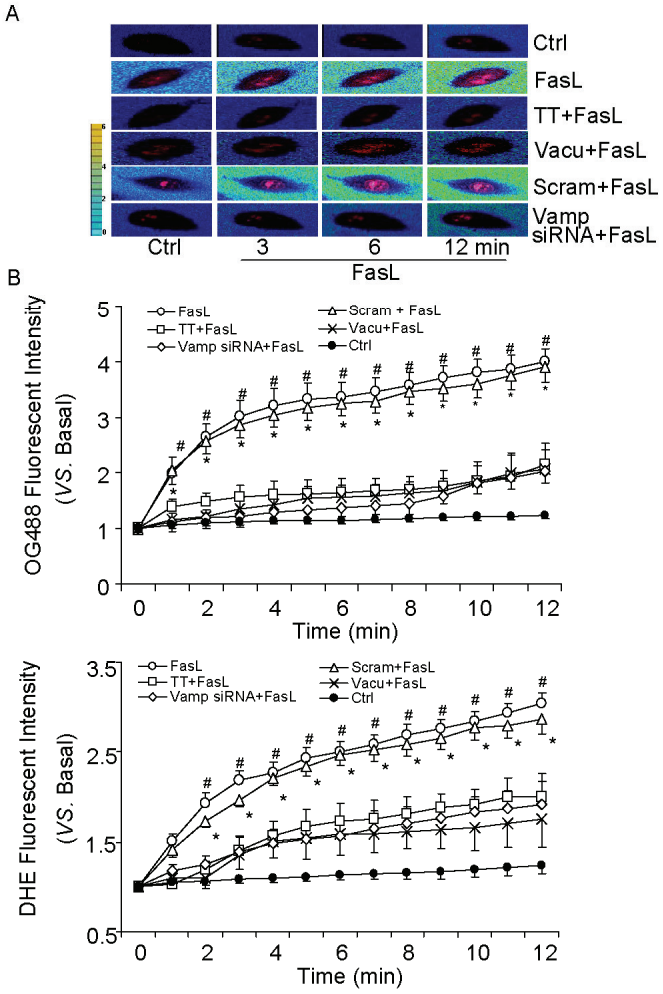

Figure 7. Effects of lysosomal fusion on extracellular pH and intracellular O_2.- production in bovine CAECs. (A) Typical merged images of OG488 and DHE fluorescence. The change of OG488 fluorescent intensity was recorded in pseudo color. (B) Summarized data showing that TT (10 nM), vacuolin-1 (10 μM) and vamp-2 siRNA significantly inhibited FasL-induced changes in extracellular pH and intracellular O_2.- production in CAECs (n=6, $^{*}P<0.05$ *vs.* Vamp-2 siRNA-treated group; $^{\#}P<0.05$ *vs.* vacuolin-1 or TT-treated group).

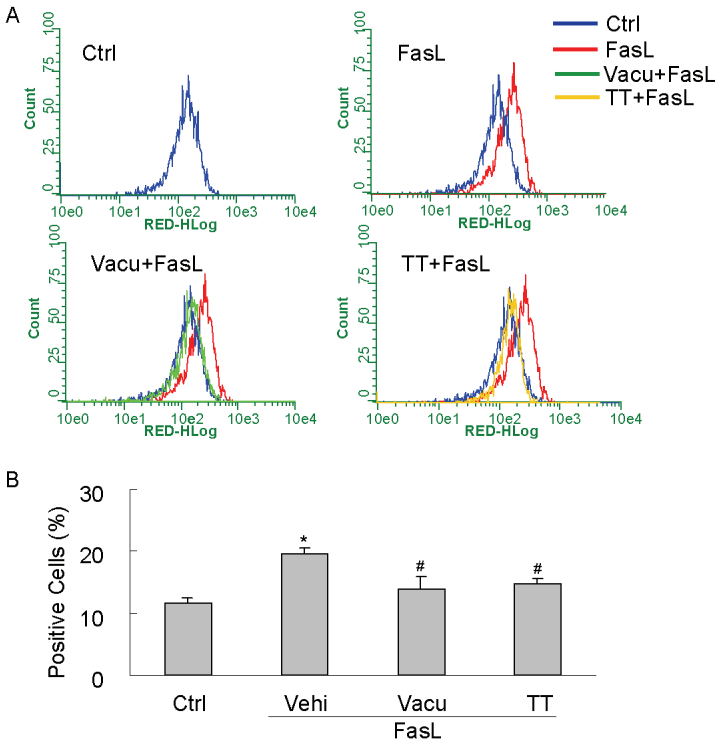

Figure 8. Measurements of H^+-ATPase translocation in bovine CAECs with flow cytometry. (A) Frequency histogram of H^+-ATPase in the membranes of control or FasL (10 ng/ml for 15 min) stimulated cells without or with TT (10 nM) or vacuolin-1(10 μM), and the overlay. (B) The percentage of H^+-ATPase positive-staining cells significantly increased in FasL-treated CAECs, which was suppressed by pre-incubation with vacuolin-1 or TT (n=6, $^*P<0.05$ *vs.* control; $^\#P<0.05$ *vs.* only FasL-treated group).

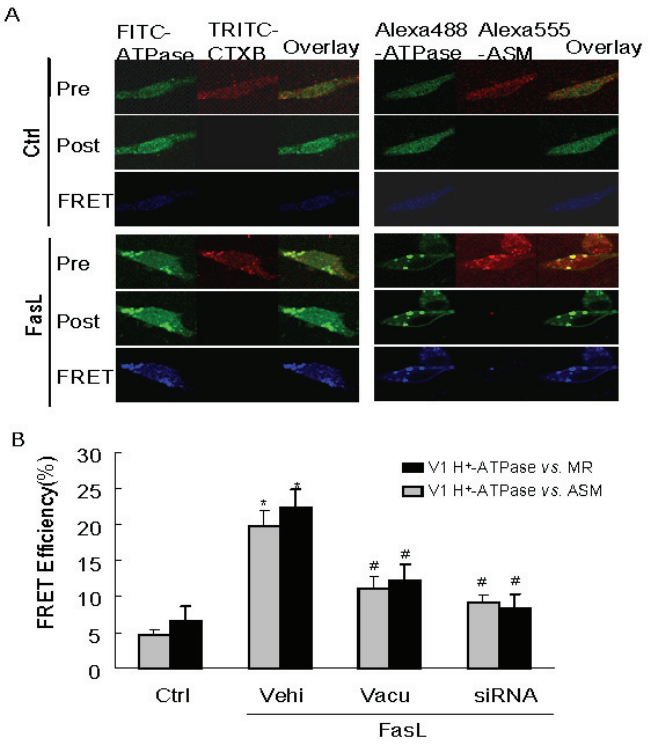

Figure 9. FRET analysis of the MR marker ganglioside GM1, H^+-ATPase, and ASM in bovine CAECs. FRET was detected using an acceptor-bleaching protocol. The blue images (representing FRET) on the bottom were obtained by subtracting a pre-bleaching image from a post-bleaching image. (A) Representative images of FRET between V1 H^+-ATPase and GM1 (CtxB labeling) or ASM. (B) Summarized results of detected FRET efficiency show that FasL significantly increased the FRET efficiency between V1 H^+-ATPase and GM1 or ASM, which was effectively inhibited by vacuolin-1(10 μM) or V1 H^+-ATPase siRNA (n=6, $^*P<0.05$ *vs.* control; $^\#P<0.05$ *vs.* only FasL-treated group).

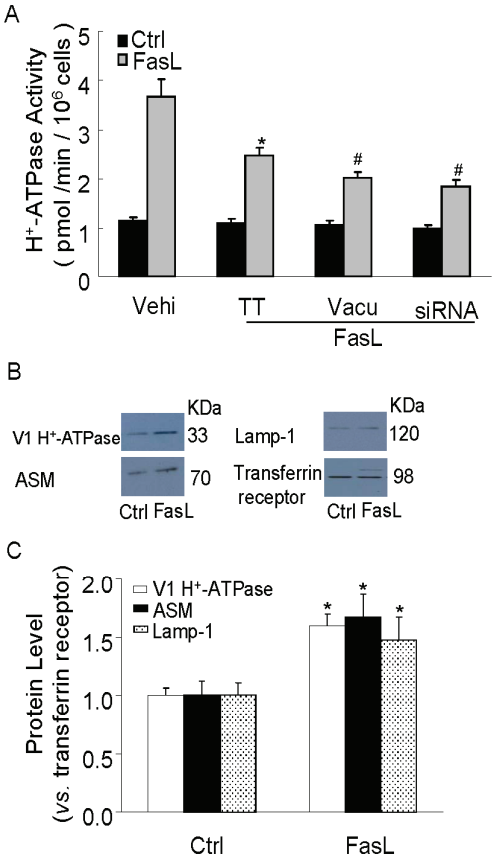

Figure 10. H^+-ATPase activity and protein expression on the cell membrane of bovine CAECs. (A) FasL (10 ng/ml) dramatically enhanced the activity of H^+-ATPase on the cell membrane of CAECs by fluorometry, which was inhibited by pretreatment of these cells with TT (10 nM), vacuolin-1 (10 μM), or V1 H^+-ATPase siRNA (n = 6, $^*P$<0.05 *vs.* control; $^\#P$<0.05 *vs.* only FasL-treated group). (B) Cell surface biotinylation assay for H^+-ATPase subunit of V1 sector protein expression in bovine CAECs. Western blot gel document presents the relative levels of V1 H^+-ATPase, ASM, lamp-1 or transferrin receptor on the cell membrane of CAECs. (C) Summarized results show that the intensity ratio of V1 H^+-ATPase to transferrin receptor increased by 59.5 % on the cell membrane in response to FasL (10 ng/ml) treatment. The intensity ratio of ASM or Lamp-1 to transferrin receptor increased by 67.1 % or 47.7%, respectively, on the cell member (n=3, $^*P$<0.05 *vs.* control).